

Easier randomizing gates provide more accurate fidelity estimation

Debankan Sannamoth,^{1, 2, *} Kristine Boone,^{3, *} Arnaud Carignan-Dugas,⁴
 Akel Hashim,^{5, 6} Irfan Siddiqi,^{5, 6} Karl Mayer,⁷ and Joseph Emerson^{1, 2, 8, †}

¹*Department of Applied Mathematics, University of Waterloo, Waterloo, Ontario N2L 3G1, Canada*

²*Institute for Quantum Computing, University of Waterloo, Waterloo, Ontario N2L 3G1, Canada*

³*Photonic Inc., Coquitlam, British Columbia, Canada*

⁴*Keysight Technologies Canada, Kanata, Ontario K2K 2W5, Canada*

⁵*Department of Physics, University of California at Berkeley, Berkeley, CA 94720, USA*

⁶*Applied Math and Computational Research Division,*

Lawrence Berkeley National Lab, Berkeley, CA 94720, USA

⁷*Quantinuum, Broomfield, CO 80021, USA*

⁸*Keysight Technologies Canada Inc., Mississauga, Ontario L5N 2M2, Canada*

(Dated: January 1, 2026)

Accurate benchmarking of quantum gates is crucial for understanding and enhancing the performance of quantum hardware. A standard method for this is interleaved benchmarking, a technique which estimates the error on an interleaved target gate by comparing cumulative error rates of randomized sequences implemented with the interleaved gate and without it. In this work, we show both numerically and experimentally that the standard approach of interleaved randomized benchmarking (IRB), which uses the multi-qubit Clifford group for randomization, can produce highly inaccurate and even physically impossible estimates for the error on the interleaved gate in the presence of coherent errors. Fortunately we also show that interleaved benchmarking performed with cycle benchmarking, which randomizes with single qubit Pauli gates, provides dramatically reduced systematic uncertainty relative to standard IRB, and further provides a host of additional benefits including data reusability. We support our conclusions with a theoretical framework for bounding systematic errors, extensive numerical results comparing a range of interleaved protocols under fixed resource costs, and experimental demonstrations on three quantum computing platforms.

I. INTRODUCTION

Randomized benchmarking [1–5] is a fundamental method in quantum computing that now comprises a broad class of methods to estimate the error rates of quantum gates [6, 7]. While these methods are often applied to estimate error rates averaged over some set or group of elementary gates, in this work we focus on interleaved benchmarking protocols which aim to estimate the error on some specific gate of interest, typically a two-qubit entangling gate such as the CNOT. The primary example of such a protocol is interleaved randomized benchmarking (IRB) [8], which is currently a standard benchmarking approach with widespread adoption across all leading experimental platforms [9–25]. The standard IRB scheme proposes implementing a reference randomized benchmarking (RB) sequence, that is, a standard RB experiment with the full Clifford group, as well as an interleaved sequence with the gate of interest interleaved between the randomizing gates. The ratio of the latter over the former is intended to provide an accurate estimate of the error on the interleaved gate alone.

In this work, we demonstrate with theoretical, numerical, and experimental evidence that the systematic uncertainty for IRB can lead to significant inaccuracy in

practice, producing not just inaccurate but even physically impossible error-rate estimates for the interleaved gate in the presence of even moderate amounts of coherent error. Fortunately, we also show that this problem can be effectively mitigated by selecting an easier-to-implement randomization group based on single-qubit gates with lower average error, notably the Pauli randomization used in cycle benchmarking (CB) [26] and the local Clifford randomization [27] used in variety of other benchmarking protocols [27, 28]. Benchmarking protocols with these simpler randomization groups have now been well-studied theoretically [27–35] and experimentally across a wide-variety of platforms [27, 28, 36–39]. In spite of the above works exploring single qubit randomization with low average error rates, there is still widespread adoption of IRB [9–25] which requires multi-qubit randomization with associated high average error rates. We show below that the dramatic inaccuracy of IRB is entirely avoidable, where the single qubit randomization of cycle benchmarking provides a far more accurate alternative for interleaved benchmarking in addition to offering a host of additional benefits at scale, including robustness under cross-talk error and data-reusability, which local clifford randomization does not provide.

Our analysis of the systematic error in interleaved benchmarking protocols builds on the systematic bounds developed in [40] which characterize how component level errors in a composition of gates can interfere coherently to give rise to significant variation in the cumulative error across a product of gates. In particular, we evaluate the

* These authors contributed equally

† Author contacts: dsannamo@uwaterloo.ca, jemerson@uwaterloo.ca

significance of this effect in different interleaved benchmarking protocols, where we demonstrate that extremely large systematic uncertainties can arise in realistic contexts. Our results counter the (incorrect) intuition that randomized sequences typically suppress coherent errors, and so destructive and constructive interference should not be a concern under randomized benchmarking. This intuition fails because for interleaved benchmarking protocol the suppression of coherence only occurs between the composed errors from the interleaved gate and the randomizing gates; coherence is not suppressed between each of these gates separately. Our work also counters the intuition that coherent (cancellation or amplification) effects for gate errors are actually rare and thus unlikely to be significant in practice. We show below that this is decidedly not the case: under typical experimental conditions, we provide both numerical and experimental evidence indicating that coherence effects can be significant enough to produce physically impossible estimates, in particular, negative error probabilities.

The manuscript is structured as follows. First, in Section II, we provide conceptual and theoretical background and establish terminology for the set of interleaved benchmarking protocols that we evaluate. In Section III A, we discuss the details about systematic bounds. In Section III B, we discuss how performing extended randomized benchmarking (XRB) to extract knowledge of the unitarity of the error along with estimates from protocols like Haar-RB and IRB helps in providing a tighter bound as compared to the systematic bounds. In Section IV, we show numerical and experimental results across three different quantum computing platforms comparing different interleaved protocols in support of our conclusions. In Appendix A, we provide a framework for constructing the self-consistent gauge under which a theoretical value can be rigorously compared to the protocol estimator, to address the gauge ambiguity of RB protocols. Finally, we conclude this work in Section V with discussions and outlook.

II. BACKGROUND: INTERLEAVED PROTOCOLS AND RANDOMIZATION VIA TWIRLING GROUPS

Interleaved benchmarking protocols aim to estimate the error on an individual gate (or cycle) of interest, rather than an average over a set of gates, and thus comprise two distinct experiments: a “reference” sequence consisting of a randomized benchmarking experiment, and an “interleaved” sequence which inserts a gate of interest between the random gates in the reference sequence.

Each reference sequence is a randomized benchmarking experiment which is an implementation of a sequence of randomly drawn gates that yields a figure of merit associated with the average error rate over that set of gates [1]. If the set forms a group, which is the case for all the

protocols we consider below, then the implemented sequence of random gates can be shown to correspond to a sequence of twirls [5]. For this reason, the randomizing gates are often assumed to be a *twirling group*, although notably this condition is not fulfilled in the single qubit randomized benchmarking scheme proposed by Knill et al [43]; see [44] for a discussion. When the twirling group is a unitary 2-design (over all qubits) [1, 2], and the error model is sufficiently gate independent, then the error on each gate is reduced to a depolarizing channel, and the error rate is a unitarily invariant quantity associated with the process fidelity of the error model [1–4]. The gate-independence condition can be relaxed and the same conclusions still hold for all practical purposes¹. In this work, we restrict our focus to two-qubit systems (generalizations to n-qubit protocols are discussed in the conclusion) and evaluate four different twirling groups, which are summarized in Table I and Fig. 1 in order of decreasing group size and complexity complexity: (Row 1) ‘Haar’ randomization based on the original RB protocol [1, 5]; (Row 2) ‘Clifford’ randomization based on the standard RB protocol [2–5], which is the standard approach for interleaved benchmarking; (Row 3) ‘Local Clifford’ randomization which was proposed in [27] and has found renewed interest recently [28, 47]; and (Row 4) ‘Pauli’ randomization which is leveraged in the cycle benchmarking [26] and cycle error reconstruction [29] protocols. Note that for the final two rows in the table we are considering reference protocols which are not unitary 2-designs across the qubits. In particular, the ‘Local Clifford’ protocol is a randomized benchmarking experiment with a group that only forms a unitary 2-design over the individual qubits (Row 3) and the ‘Pauli’ protocol (Row 4) is a randomized benchmarking experiment which only forms a unitary 1-design over the individual qubits. In these two protocols, the experimental decay nonetheless produces an estimator of the average process fidelity, as described in the final column. The circuits for the benchmarking experiments under each of the reference protocol groups are shown in the first column of Fig. 1.

The interleaved sequences interleave a gate of interest \mathcal{G} between the randomizing (i.e., twirling) gates of the associated reference protocol. The circuits for interleaved benchmarking experiments under each of the reference protocol groups are shown in the second column of Fig. 1. We have adopted a compact notation where we specify the reference and interleaved protocols with the same label but denote the interleaved gate \mathcal{G} in parentheses, and denote the lack of an interleaved as an identity gate \mathcal{I} in parentheses, highlighting that the reference protocol

¹ Under gate-dependent error models, the above conclusions hold except for the caveat that the error model corresponds to the average error ‘between the gates’ of the randomized sequence [45] rather than the error ‘on’ each gate, resolving the concern raised in [46]. See Appendix for further details.

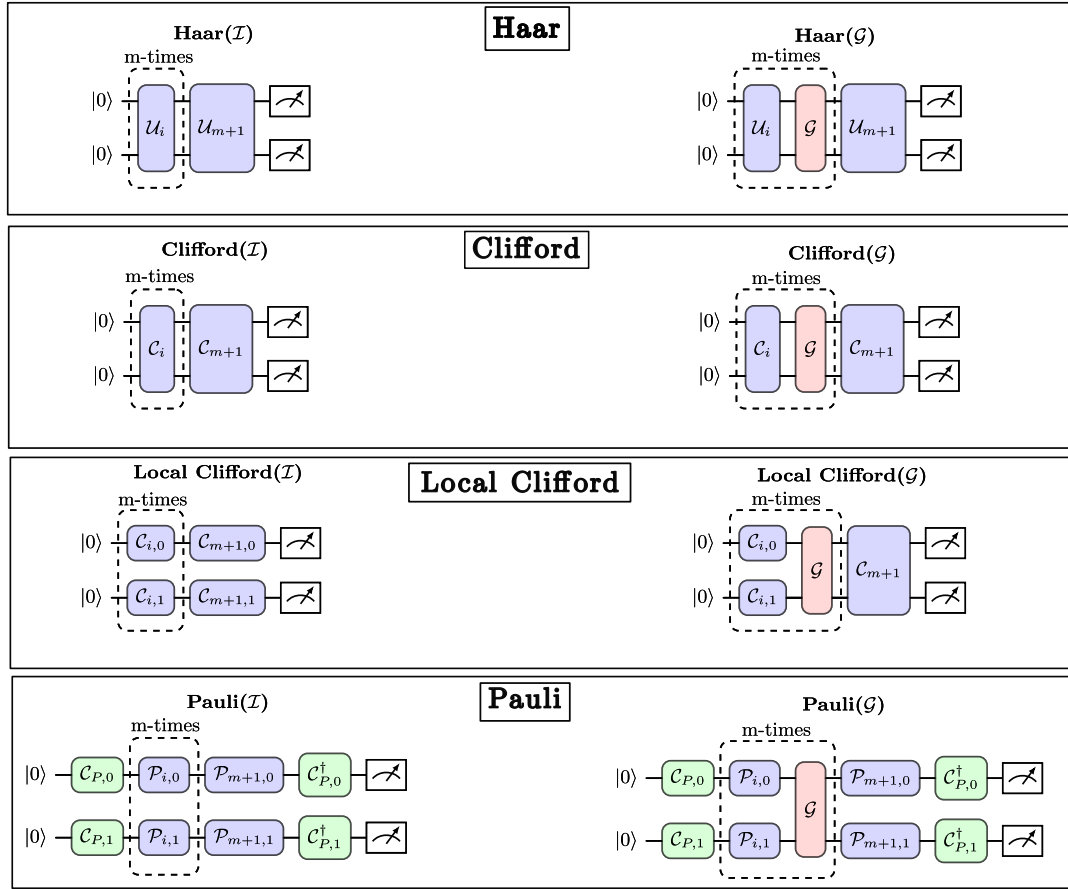


FIG. 1. Circuits for interleaved protocol pairs for each of four different protocols with distinct randomizing/twirling groups which we label: Haar, Clifford, Local Clifford and Pauli; see also their descriptions in Table 1. In each pair, the interleaved and reference protocols are denoted by the twirling group name followed by (\mathcal{G}) and by (\mathcal{I}) , respectively, which specifies where the gate \mathcal{G} or no gate (viz \mathcal{I}) is interleaved in between the twirling gates. Please note that the notation (\mathcal{I}) does not mean that there is an identity gate or delay inserted in lieu of the interleaved gate, but denotes that the reference protocol is identical to the interleaved protocol except that it has no interleaved gate. For Haar, the twirling gates \mathcal{U}_i are drawn uniformly at random from $\text{SU}(4)$ according to the Haar measure and \mathcal{U}_{m+1} denotes the correction gate $\text{SU}(4)$ required in motion reversal circuits per the original RB protocol [1]. For Clifford, the twirling gates \mathcal{C}_i are drawn at random from \mathbb{C}_2 where \mathbb{C}_2 is the 2-qubit Clifford group and \mathcal{C}_{m+1} is the correction gate [3]. For Local Clifford, twirling gates are drawn uniformly at random from the tensor product of 1-qubit Clifford groups $\mathbb{C}_1^{\otimes 2}$ with $\mathcal{C}_{i,j} \in \mathbb{C}_1$ at time step i on qubit j , $\mathcal{C}_{m+1,j}$ are the single-qubit correction gates and \mathcal{C}_{m+1} is the 2-qubit correction gate required for motion reversal of the interleaved sequence [28, 41, 42]. For Pauli, twirling gates are drawn uniformly at random from the tensor product of 1-qubit Pauli group $\mathbb{P}_1^{\otimes 2}$ with $\mathcal{P}_{i,j} \in \mathbb{P}_1$ at time step i on qubit j , where in these circuits $\mathcal{C}_{P,j}$ are local Clifford operators used only for generating the state preparation and measurement in the $+1$ eigen state of a random Pauli P , which is the cycle benchmarking scheme proposed in [26].

is equivalent to the corresponding interleaved protocol when the interleaved gate is the identity gate. To be clear, this notation does not imply inserting an identity gate or a delay equivalent to the identity channel in lieu of the interleaved gate, but simply means that the reference protocol is associated with the absence of an interleaved gate.

The composition of the interleaved gate with an adjacent randomizing gate is called the ‘dressed gate’. The interleaved sequence actually directly estimates the error on this composition and the error rate on the interleaved gate is then inferred via an estimator, as discussed in the next section. That is, the interleaved protocol estimates an average error rate associated with the cumulative error on the dressed gate, and the process infidelity of the

interleaved gate is then inferred by comparing the two measured error rates, as described in the next section. The central problem that we describe and solve in this paper is that the inferred error on the interleaved gate can vary unpredictably and dramatically when the errors on the randomizing gate and interleaved gate are coherent, but this can be mitigated when the error rate of the reference randomizing group is significantly lower than the interleaved gate.

While IRB using the two-qubit ‘Clifford’ group is the standard approach and cycle benchmarking using the single qubit ‘Pauli’ group is the leading alternative, we also have proposed an interleaved benchmarking protocol based on the based on ‘Haar’ randomization in Row 1 for two reasons: (i) the Haar twirl is the only twirl that nat-

urally allows for interleaved gates that are arbitrary non-Clifford gates, and thus enables cross-platform comparisons that include platforms using non-Clifford gates such as Google’s fSim gate [48], and (ii) considering the ‘Haar’ twirl (which requires 3 CNOTs on average compared to 1.5 CNOTs for ‘Clifford’) also allows us to explore inaccuracy as a function of varying circuit complexity. We also included ‘Local Clifford’ due to the recent benchmarking proposal in [49]. ‘Local Clifford’ has a larger group size (24^n , which can be reduced to 12^n) than the ‘Pauli’ group (4^n), and can have greater circuit complexity depending on the compilation scheme and primitive gate set. In this work we considered a compiling scheme such that these two single qubit randomization groups have the same circuit complexity (see IV A for further details).

III. THEORY

The central quantity of interest is the process fidelity of an implemented gate, either averaged over a set of gates or associated with a target gate of interest, relative to its ideal counterpart. The process fidelity gives the same information as the average gate fidelity which only differ by dimensional factors [51]. Both of these fidelities are standard figures of merit because they can be defined as invariant quantities associated with the average overlap over a natural set of operators [52].

The process infidelity of a quantum error channel \mathcal{E} is most easily computed from the Pauli Transfer Matrix, which is the Liouville representation of \mathcal{E} in the Pauli basis and is denoted by $[\mathcal{E}]$, such that

$$\epsilon^{\mathcal{E}} = 1 - \frac{\text{Tr}[\mathcal{E}]}{d^2} \quad (1)$$

where d is the dimension of the Hilbert space.

In the context of our work, we are interested in the process infidelity of the error map \mathcal{E} that is associated with an ideal unitary gate U relative to its imperfect implementation, which can be written as $\mathcal{E}_U = U \circ \mathcal{E}$. So we let $\epsilon^{\mathcal{E} \circ \mathcal{F}}$ denote the process infidelity associated with the error on the *dressed gate*, which consists of a twirling gate combined with the interleaved gate, and $\epsilon^{\mathcal{E}}$ denote the process infidelity associated with the errors on the cycles of randomizing gates.

Interleaved protocols aim to estimate the process infidelity of the error on the interleaved gate alone, but this cannot be uniquely determined from $\epsilon^{\mathcal{E} \circ \mathcal{F}}$ and $\epsilon^{\mathcal{E}}$ for general error models. Thus interleaved protocols require an estimator for process infidelity of the error on interleaved gate $\hat{\epsilon}^{\mathcal{F}}$, which can be obtained by relating $\epsilon^{\mathcal{E} \circ \mathcal{F}}$ with $\epsilon^{\mathcal{E}}$ as follows

$$\hat{\epsilon}^{\mathcal{F}} = 1 - \frac{1 - \epsilon^{\mathcal{E} \circ \mathcal{F}}}{1 - \epsilon^{\mathcal{E}}}. \quad (2)$$

For depolarizing errors, this estimator becomes exact as the error rate approaches zero, but for more general errors, with a coherent component, this estimator is subject

to significant inaccuracy, and the extent of this inaccuracy is the main focus of our study. We note here that this estimator formula differs (albeit negligibly) from the estimator in the original interleaved proposal in [8], which is expressed in terms of the decay parameter ‘ p ’ for randomized benchmarking. Our formulation of the estimator is more general as it allows for a unified approach that applies to a general class of interleaved benchmarking schemes with twirling groups other than Clifford, including cases, in particular the *Pauli* case for cycle benchmarking, in which no single decay parameter exists. In Appendix B, we show that the difference between the two approaches is asymptotically negligible in the low error regime, and practically negligible differences under typical error rates for the numerical and experimental data in this paper.

A. Systematic Uncertainty for Interleaved Benchmarking

The estimator of the process infidelity of the interleaved gate is inferred from the ratio of the estimators of the two sequences, as shown in Eqn. 2. Any such estimator is subject to a *systematic uncertainty* which arises because the coherence in the errors at the component level can constructively and destructively interfere between adjacent gates in the gate sequences, producing a wide range of possible outcomes. The (in)accuracy of this inference is quantified by the following inequality: for two quantum error channels \mathcal{E} and \mathcal{F} , expressed in terms of their process infidelities, we have [40]

$$\begin{aligned} & | -\epsilon^{\mathcal{F}} + \epsilon^{\mathcal{E} \circ \mathcal{F}} + \epsilon^{\mathcal{E}} - 2\epsilon^{\mathcal{E} \circ \mathcal{F}}\epsilon^{\mathcal{E}} | \\ & \leq 2\sqrt{(1 - \epsilon^{\mathcal{E} \circ \mathcal{F}})(1 - \epsilon^{\mathcal{E}})\epsilon^{\mathcal{E} \circ \mathcal{F}}\epsilon^{\mathcal{E}}}. \end{aligned} \quad (3)$$

The systematic uncertainty associated with the estimator in Eqn. 2 due to Eqn. 3 can be re-expressed as

$$\begin{aligned} \epsilon^{\mathcal{F}} & \geq \epsilon^{\mathcal{E} \circ \mathcal{F}} + \epsilon^{\mathcal{E}} - 2\epsilon^{\mathcal{E} \circ \mathcal{F}}\epsilon^{\mathcal{E}} \\ & - 2\sqrt{(1 - \epsilon^{\mathcal{E} \circ \mathcal{F}})(1 - \epsilon^{\mathcal{E}})\epsilon^{\mathcal{E} \circ \mathcal{F}}\epsilon^{\mathcal{E}}} \end{aligned} \quad (4a)$$

$$\begin{aligned} \epsilon^{\mathcal{F}} & \leq \epsilon^{\mathcal{E} \circ \mathcal{F}} + \epsilon^{\mathcal{E}} - 2\epsilon^{\mathcal{E} \circ \mathcal{F}}\epsilon^{\mathcal{E}} \\ & + 2\sqrt{(1 - \epsilon^{\mathcal{E} \circ \mathcal{F}})(1 - \epsilon^{\mathcal{E}})\epsilon^{\mathcal{E} \circ \mathcal{F}}\epsilon^{\mathcal{E}}} \end{aligned} \quad (4b)$$

Of course, these estimators are subject to the usual statistical uncertainty obtained using standard methods of error propagation, in addition to the above systematic uncertainty. In the following figures, these two uncertainties are distinguished by solid vs dashed lines.

B. Unitarity and XRB bounds

One can reduce the size of the systematic uncertainty identified in Eqn. 4 by performing an independent measurement of the degree of coherence of the method via

Twirling/Randomizing Group			Interleaved Protocol Pair		Initial State(s)	Estimator for Process Infidelity
Label	Symbol	Description	Reference	Interleaved		
Haar	$\mathbb{SU}(4)$	Haar-random 2-qubit unitaries	Haar(\mathcal{I}) (= Haar RB [1])	Haar(\mathcal{G}) (new)	$ 0\rangle^{\otimes 2}$	$\hat{\epsilon} = \epsilon$ [1]
Clifford	\mathbb{C}_2	Random 2-qubit Clifford gates	Clifford(\mathcal{I}) (= Standard RB [3])	Clifford(\mathcal{G}) (= IRB [8])	$ 0\rangle^{\otimes 2}$	$\hat{\epsilon} = \epsilon$ [1–4, 8]
Local Clifford	$\mathbb{C}_1^{\otimes 2}$	Random 1-qubit Clifford gates	Local Clifford(\mathcal{I}) (= Simultaneous single-qubit RB [50])	Local Clifford(\mathcal{G}) (= Direct RB [28, 41, 42])	$ 0\rangle^{\otimes 2}$	$\hat{\epsilon} \approx \epsilon$ asymptotically [41, 42]
Pauli (=CB [26])	$\mathbb{P}_1^{\otimes 2}$	Random Pauli gates	Pauli(\mathcal{I}) (= CB with \mathcal{I})	Pauli(\mathcal{G}) (= CB with \mathcal{G})	Pauli eigenstates	$\hat{\epsilon} = \epsilon + \mathcal{O}(\epsilon^2)$ [26]

TABLE I. Summary of the interleaved protocol pairs for different twirling groups, the circuits for which are shown in Fig. 1. Protocols are listed in order of decreasing circuit complexity (and group size) for the randomizing gates, with the first two rows requiring multi-qubit (entangling gates) and the last two rows requiring only single qubit gates. See text and caption to Fig. 1 for further details.

protocols such as extended-RB (XRB)[53]. It is a modification to RB style experiments where correction operation at the end of the sequence is replaced with state tomography. The basic idea is that coherent errors preserve the purity of the state, where purity is defined as $\text{Tr}(\rho^2)$. For pure states, $\text{Tr}(\rho^2) = 1$ while for mixed state $\text{Tr}(\rho^2) < 1$. Starting with a pure state, the coherent errors perform a rotation of the pure state on the Bloch sphere, keeping it a pure state. The quantity of interest that we measure using XRB is called *unitarity* which is a quantifier of the coherence of the error acting on the gates of the experiments. Mathematically, we can define *unitarity* as

$$u(\mathcal{E}) = \frac{1}{d-1} \int d\psi \|\mathbf{n}(\mathcal{E}|\psi\rangle\langle\psi|) - \mathbf{n}(\mathcal{E}(I/d))\|^2 \quad (5)$$

where \mathbf{n} denotes the generalized d -dimensional Bloch vector and $\|\mathbf{n}(\rho)\|^2$ denotes the Euclidean norm. We can instantly see a direct relationship between purity of a state and the Euclidean norm of the Bloch vector, which for a single-qubit is

$$\begin{aligned} \text{Tr}(\rho^2) &= \frac{1}{4} \left[\text{Tr}(I_2) + 2\text{Tr}(n_x X + n_y Y + n_z Z) \right. \\ &\quad \left. + \text{Tr}((n_x^2 + n_y^2 + n_z^2)I_2) \right] \quad (6) \\ &= \frac{1}{2} [1 + \|\mathbf{n}(\rho)\|^2] \end{aligned}$$

Another equivalent definition of unitarity is

$$u(\mathcal{E}) = \frac{1}{d^2-1} \text{Tr}[\mathcal{E}_u^\dagger \mathcal{E}_u] \quad (7)$$

where \mathcal{E}_u denotes the $(d^2 - 1) \times (d^2 - 1)$ unital block of the CPTP map \mathcal{E} in the Liouville representation.

For an in-depth description of the protocol, see [53]. Once we have the *unitarity*, we can provide a tighter bound on the systematic uncertainty in Eqn. 3. For distinguishability from systematic bounds, we would call these bounds *XRB bounds*, which are given as

$$\left| p(\mathcal{Y}) - \frac{p(\mathcal{X}\mathcal{Y})p(\mathcal{X})}{u(\mathcal{X})} \right| \leq \sqrt{1 - \frac{(p(\mathcal{X}))^2}{u(\mathcal{X})}} \sqrt{1 - \frac{(p(\mathcal{X}\mathcal{Y}))^2}{u(\mathcal{X})}} \quad (8)$$

where p is the depolarizing parameter in RB experiments.

C. Defining the relevant fidelity based on the effective error model between the gates

In the context of all numerical studies of benchmarking experiments, there is an ambiguity in computing the fidelity of the operationally relevant error model [45, 46, 54]. This arises because an average fidelity computed naively based on the average ‘error-on-the-gate’ may not be relevant when there can be systematic cancellation of error between a gate and the subsequent gate. This is sometimes stated as a dependence on a choice of gauge, where the appropriate gauge itself depends on the randomizing group. Thus, to define the relevant fidelity in a rigorous way, a method is required to identify the self-consistent gauge (SCG) associated with each randomizing group. To compare the accuracy of these benchmarking protocols to a rigorous theoretical fidelity

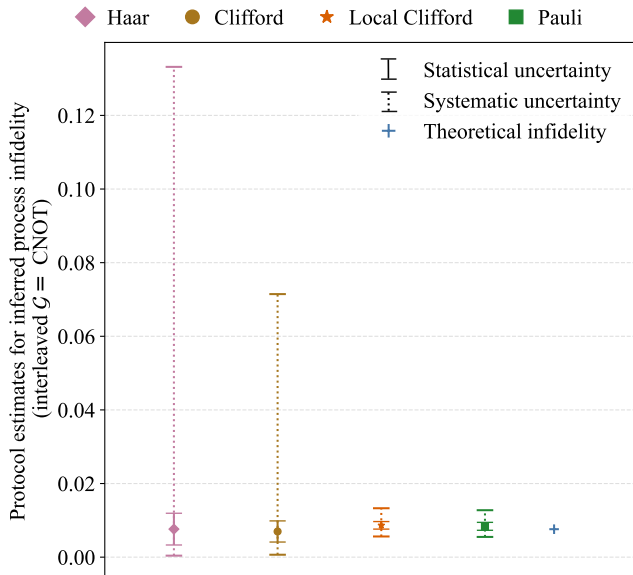


FIG. 2. Comparison of systematic uncertainty as a function of the different twirling groups defined in Table I, showing that Pauli and Local Clifford twirling groups have the smallest systematic uncertainties, while keeping the number of shots fixed. The error model comprises coherent error on the two-qubit gates of the form $e^{i\theta_2 ZZ}$ with $\theta_2 = 10^\circ$ and coherent error on the single-qubit gates of the form $e^{i\theta_1 Z}$ with $\theta_1 = 1^\circ$. The theoretical infidelity is the obtained using Eqn. 1 under a naive (identity) choice of gauge. Even though Local Clifford group is larger than Pauli group, due to our chosen decomposition and error model on single-qubit gates as detailed in IV A, both have almost same error magnitude and provides almost the same accuracy in the estimate.

in numerical studies, we also introduce a protocol for finding the gauge associated with any gate-dependent error model for each randomized benchmarking sequence. We develop this framework in the Appendix A, and provide a comparison of the SCG fidelity for the ‘error-between-the-gates’ and the theoretical fidelity associated with the errors ‘on’ the gates in the results. As a corollary, we find that for realistic error models and randomizing groups of interest, the differences between SCG fidelities and the theoretical fidelity is negligible.

IV. RESULTS

A. Numerical results

We now present numerical simulations to address the central questions motivating this work. We first demonstrate in Fig. 2 how dramatically the systematic uncertainties from Eqn. 4 vary under the four different pairs of benchmarking protocols and their associated twirling groups (see Fig. 1 and Table I). The error model comprises coherent error on the two-qubit gates of the form $e^{i\theta_2 ZZ}$ with $\theta_2 = 10^\circ$ and coherent error on the single-qubit gates of the form $e^{i\theta_1 Z}$ with $\theta_1 = 1^\circ$. The figure

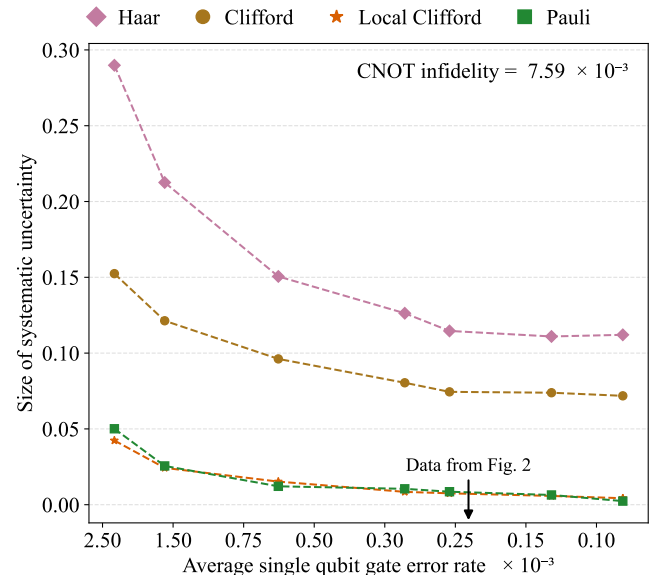


FIG. 3. Numerical plot showing the size of the systematic uncertainty for varying average single-qubit gate error rate. The error model is the same as the one used in Fig. 2 with θ_2 fixed at 10° and varying θ_1 so as to vary the average single-qubit gate error rate along the x-axis. The other simulation parameters are the same as Fig. 2 which is a typical instance of this plot.

demonstrates that the magnitude of systematic uncertainty varies substantially across protocols with different twirling groups, where protocols employing twirling groups with more total error, such as Haar and Clifford, which require two qubit gates, exhibit significantly larger systematic uncertainties than those based on minimal twirling groups, including Local Clifford and Pauli. Notably, despite the Local Clifford being strictly larger than the Pauli group, the two yield nearly identical systematic uncertainties in our simulations. This similarity in performance is because we implement all single qubit gates via the decomposition $Z(\theta)X(\pi/2)Z(\omega)X(\pi/2)Z(\phi)$ decomposition [55, 56], and assume that only the $X(\pi/2)$ gates have error where the Z rotations are error free as they can be implemented experimentally virtually in software. As a result of this approach, single-qubit Pauli gates and single-qubit Clifford gates have almost the same average error rates. The number of shots used is $s = 1500$ which for the Pauli twirling group is 100 randomizations distributed equally across 15 input states. For $\text{Haar}(\mathcal{G})$, $\text{Haar}(\mathcal{I})$, $\text{Clifford}(\mathcal{G})$ and $\text{Clifford}(\mathcal{I})$ the cycle depths $m \in \{4, 6, 8, 12, 14\}$. For $\text{Local Clifford}(\mathcal{G})$, $\text{Pauli}(\mathcal{G})$ $m \in \{4, 8, 12, 16, 20\}$ and for $\text{Local Clifford}(\mathcal{I})$, $\text{Pauli}(\mathcal{I})$ $m \in \{4, 8, 12, 20, 30\}$.

In Fig. 3 we explore how the size of the systematic error varies as we decrease the error rate on the single-qubit gates. The trend confirms that systematic error decreases as the error rate on the twirling gates decreases, and again shows that protocols with larger twirling groups (and more total error) consistently exhibiting significantly larger systematic uncertainties than those employ-

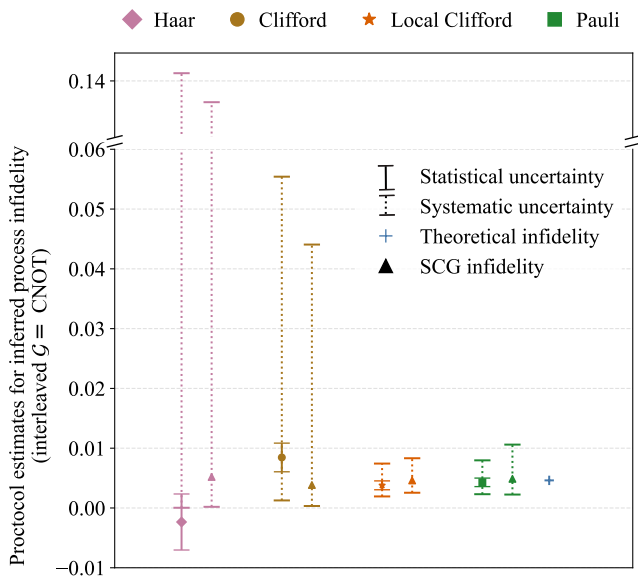


FIG. 4. Numerical plot highlighting the importance of systematic uncertainties for a natural (overrotation) coherent error model, where we see that the theoretical infidelity value is well outside the statistical bar of the estimates of the protocols such as Haar and Clifford, but is within the systematic bound. This figure also highlights how interference of errors can lead to negative (unphysical) estimate of process infidelity, as is observed for the Haar protocol, an effect we also see experimentally as described in the next section. The overrotation error model is of the form $U^{1+\delta}$ where U is the target unitary, with $\delta = 0.05$ for two-qubit gates and $\delta = 0.01$ for single-qubit gates. Other simulation parameters are the same as in Fig. 2. The triangles beside each estimate are the infidelities computed using the self-consistent gauge (SCG) for each twirling group; we see that the SCG yields an almost negligible difference to the naive “error on the gate” method for computing the theoretical infidelity. See Appendix A for more details on how to construct the self-consistent gauge.

ing minimal twirling groups.

We now demonstrate the practical importance of accounting for the systematic error bounds, where in the presence of simple coherent errors, statistical error bars alone are insufficient and systematic effects can dominate the interpretation of benchmarking estimates. Fig. 4 is a repetition of the numerical simulations from Fig. 2 but under an overrotation error model of coherent errors, for which the noisy implementation of any unitary U is $\tilde{U} = U^{1+\delta}$. This figure highlights the critical role of the systematic uncertainty, because we observe clear signatures of coherent interference between the twirling gates and the interleaved gate: the theoretical infidelity lies outside the statistical error bars for both of the Haar and Clifford protocols. Moreover, in the case of the Haar protocol, this interference drives the estimated process infidelity to a negative value, which is a physically impossible estimate. As we will show in the next section, physically impossible estimates of the fidelity (due to coherent error cancellation) is not a contrived occurrence in our numerics; on the contrary this is an effect we also observed experimentally.

We can however contrive adversarial coherent error models that show the extent of the systematic error that can occur in practice. For the standard IRB protocol, i.e., the Clifford protocol, we fix the error on the interleaved CNOT gate to be $e^{i\theta XZ}$, and consider two different error models for the random two-qubit Clifford gates: $e^{i\theta YY}$ or $e^{-i\theta YY}$. As shown in Fig. 5, whereas the reference RB experiment, i.e., Clifford(\mathcal{I}), has the same process infidelity in both the cases, the inferred process infidelity for the interleaved gate differs dramatically due to constructive (amplification of error) vs destructive (cancellation of error) coherence. This error model is of course contrived so that under conjugation by the CNOT gate, a YY error transforms into $-XZ$. Consequently, depending on the relative sign, the coherent errors on the interleaved and twirling gates can either add constructively or cancel destructively. In the case, where the errors cancel, we yet again obtain a negative, and therefore unphysical, estimate of the process infidelity of the interleaved CNOT gate. While similar interference can in principle occur in other benchmarking protocols, the effect is far less pronounced when Local Clifford or Pauli groups are used, since errors on these twirling gates are unlikely to match the structure and magnitude of the error on a two-qubit CNOT. Minimal twirling groups such as the Local Clifford and Pauli groups exhibit substantially lower systematic uncertainty and exhibit much more limited sensitivity to these extreme effects of coherent interference, making them far more reliable for estimating gate performance.

All numerical simulations in this work are performed under a fixed resource budget, with the total number of shots s across all the protocols set equal to ensure an even-handed comparison. We are working in the *single-shot-per-randomization* limit, where each shot of an experiment corresponds to a new, distinct random circuit. An experimental demonstration of this limit where each shot is a new randomization has been shown in [57]. Since the Pauli and Local Clifford twirling groups do not form a unitary 2-design [2], we use different state preparation, measurement and decay curve fitting strategy as described in [26, 28]. For instance in Pauli(\mathcal{G}) and Pauli(\mathcal{I}) as described in Table I and Fig. 1, we need to prepare the state in K different +1 eigenstate of the Paulis where each of the input state is assigned $s' = \frac{s}{K}$ shots such that the total number of shots across each all the experiments remain s and we extract the fidelity decay parameter corresponding to each Pauli of interest. Pauli(\mathcal{G}) and Pauli(\mathcal{I}) are equivalent to the extension of Cycle Error Reconstruction (CER) proposed in [31] where the number of repetitions of the hard cycle is 0 and 1 respectively. The general extension employing multiple values of hard gate repetitions provides more statistically stable fidelity estimates, but is more resource-intensive. For Local Clifford(\mathcal{I}), two single-qubit fidelity decay parameters are obtained, one for each qubit.

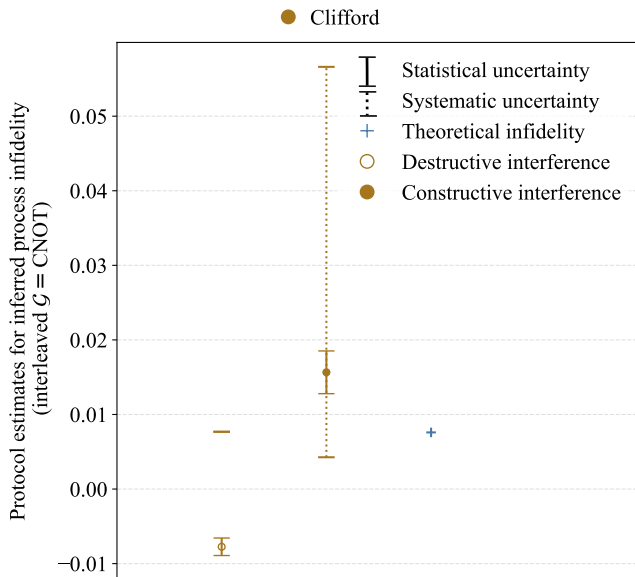


FIG. 5. Numerical plot showing how coherent errors between random twirling gates and fixed hard gate can constructively and destructively interfere to give entirely different infidelity estimates using Clifford protocols. For the destructive interference shown by yellow open circle we use the coherent error model of the form $e^{i\theta YY}$ and for constructive interference shown by yellow closed circle we use $e^{-i\theta YY}$ on the random Clifford gates and $e^{i\theta XZ}$ on the interleaved CNOT gates with $\theta = 10^\circ$. The process infidelity of the reference experiments corresponding to both error models of the form $e^{i\theta YY}$ and $e^{-i\theta YY}$ are same as it only depends on the magnitude of θ . Notice that in the destructive interference case the inferred interleaved CNOT is negative (unphysical) with the lower and upper systematic bound collapsing to a single value using Eqn. 4. We also observe similar unphysical estimate due to interference of coherent errors in experimental data, as shown in Fig. 6.

B. Experimental results

We now present experimental results for the three of the interleaved benchmarking protocols across three experimental platforms with $\mathcal{G} = \text{CNOT}$ as the interleaved gate. The experimental data are shown in Fig. 6. The first two columns of experimental data were performed on the Advanced Quantum Testbed (AQT) from Lawrence Berkeley National Laboratory, an 8 qubit device with 4 operational qubits at the time of implementation. The AQT superconducting system used for the experiments is the same as the one used in [36]. These results, repeated for two different pairs of qubits, illustrate that cycle benchmarking with Pauli twirling [26] consistently provides a much more reliable estimate of process infidelity with significantly reduced systematic uncertainty compared to the standard IRB protocol based on Clifford randomization. Indeed, we see that under the actual experimental errors (not engineered errors) the interleaved protocol with the Haar twirling group can actually produce negatively valued estimated for the infidelity of the interleaved gate, as we also observed in the numerical

simulations of the previous section.

The final three columns provide a further set of experiments designed to illustrate these effects across two other experimental platforms. The cross-platform results consistently show large the systematic uncertainties for infidelity estimates under both Haar and Clifford randomization compared to the more accurate estimates through the Pauli randomization used in cycle benchmarking [26]. These results also explore the reduction in uncertainty that is achievable via benchmarking the degree of coherence in the error via the XRB protocol. The results also highlight that even the tighter XRB bounds are still larger than the systematic bounds of CB and fall short of its greater accuracy. For the cross-platform benchmarking we focused on the Haar protocol because it is the unique protocol that can accommodate cross-platform comparisons with inequivalent and non-Clifford interleaved gates. In addition to the AQT results, the other two platforms were a superconducting device from IBM (Yorktown), a 5 qubit device, and an ion-trap device (H0), a 6 qubit device from Honeywell Quantum Solutions, now Quantinuum. It is important to note that the results from these devices were from late 2019 and therefore do not showcase how well their premium devices currently operate. The H0 device was a 6 qubit trapped-ion quantum processor using the quantum charge coupled device (QCCD) architecture [58]. On H0, qubits are encoded in hyperfine levels of Yb^+ ions, which are trapped by AC electric fields in a surface ion-trap. Single-qubit and two-qubit gates are performed in one of two separated gate zones, containing up to two qubits at a time, and all-to-all qubit connectivity is achieved by shuttling ions between zones.

V. CONCLUSION

In this work we compared the accuracy of four interleaved benchmarking protocols defined by distinct choices of randomizing gates, including most notably the widely-adopted interleaved randomized benchmarking (IRB) protocol based on the standard randomized benchmarking with the multi-qubit Clifford operations, and the more recently proposed cycle benchmarking (CB) protocol which leverages local randomization with single qubit Pauli gates. We demonstrated experimentally on multiple platforms, and also numerically under a family of coherent error models and error strengths, that the standard approach of IRB is subject to a very large systematic uncertainty that makes the protocol highly inaccurate for estimating the infidelity of an interleaved gate in the presence of coherent errors. Fortunately, we found that this inaccuracy is largely mitigated when cycle benchmarking is adopted for estimating the infidelity of an interleaved gate and more generally showed that the accuracy of interleaved protocols improves as a function of decreasing error on the choice of randomizing gates.

We also considered the protocol for bounding the

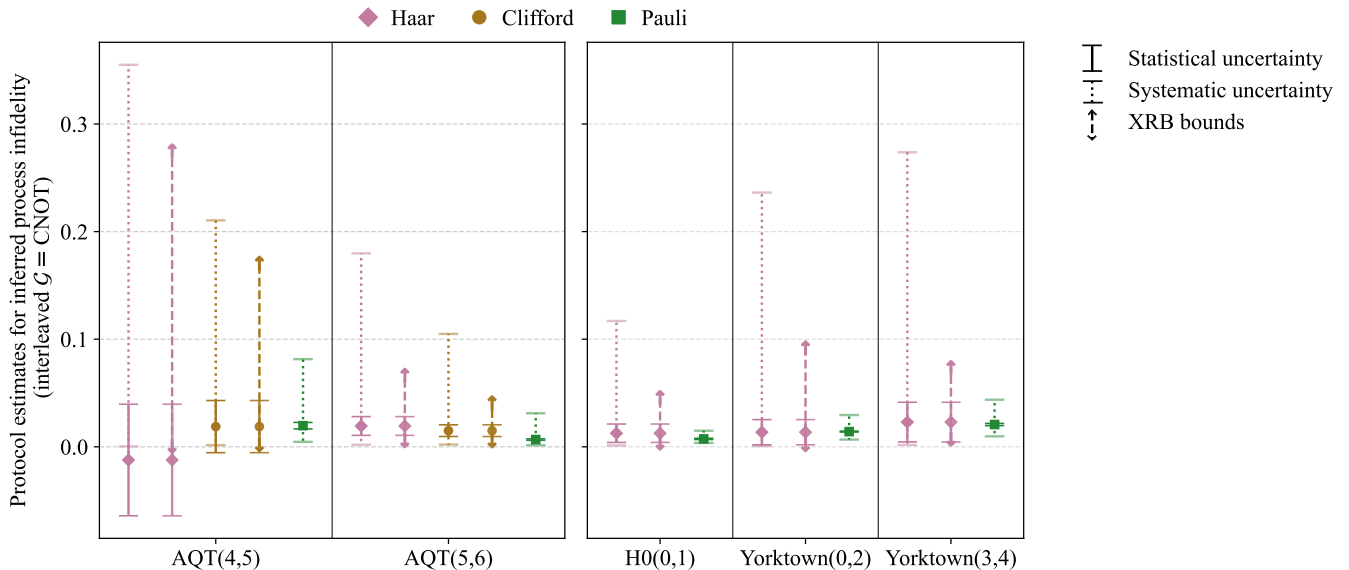


FIG. 6. Experimental data across multiple platforms illustrating the significant systematic uncertainties in estimated infidelities of interleaved gates, and showing that the accuracy of interleaved benchmarking improves under randomizing gates with lower error rates: the Pauli randomization in cycle benchmarking [26] shows significantly lower uncertainty than standard IRB with either Clifford or Haar randomization. The experimental data also show how estimating the unitarity can help reduce the systematic uncertainty as detailed in section III B (XRB bounds), however this reduced bound still remains substantially larger than the systematic uncertainty from Pauli randomization under cycle benchmarking. Also notable in the first column (AQT(4,5)), the IRB protocol with Haar randomization yields a negative valued (unphysical) estimates of the process infidelity due to destructive interference, as also discussed in the numerical simulations. Details on the experimental platforms are present in section IV B of the main text.

amount of coherent errors on the Clifford gate set, the so-called unitarity of the errors, but found that even when IRB is supplemented by this technique, it still dramatically underperforms the accuracy of cycle benchmarking. Our conclusion is that highest accuracy method for calibration and benchmarking of an interleaved gate is achieved by leveraging randomizing gates with the lowest error rates, which for most platforms implies leveraging single qubit randomizing gates such as the Pauli gates considered in cycle benchmarking or the local Clifford gates that generate a variant of direct RB. However, it should be noted that when generalizing these conclusions to benchmarking the infidelity of cycles of hard gates, such as parallel CNOT or CPhase gates, then twirling with local Cliffords (called simultaneous direct RB, or SDRB) overcounts errors due to inter-gate crosstalk [28, 49], which is a distinct source of bias and systematic error (even in the case of incoherent error) that CB entirely avoids. Thus in this context CB would be more reliable even if it shares the same level of systematic uncertainty due to coherent errors in the randomizing gates as SDRB. But we leave a detailed analysis of this for future work.

Finally we observe that cycle benchmarking also provides the additional benefit of matching the circuit structure and characterizing the experimentally relevant gate error rates that would be observed in algorithm or error-correction performance under randomized compiling [36, 37, 59–69]. And, moreover, the implementa-

tion of CB shares much of the same data set as required for partial or complete error reconstruction via the CER scheme [29], and thus CB results can be further leveraged to provide much more detailed information about the error model, at little to no additional resource cost. CB can also be easily implemented with hardware efficient randomization offering significantly reduced latencies [57].

The takeaway from our analysis is that CB is the most accurate and resource efficient scheme for fast, high-fidelity gate calibration and benchmarking under minimal error model assumptions with the added benefit of significant data re-usability.

ACKNOWLEDGMENTS

We thank Joel Wallman, Nicholas Fazio, Matthew A. Graydon, Ian Hincks, Egor Ospadov, Dar Dahlen for helpful discussions. Numerical simulations were performed using True-Q software [30]. We acknowledge financial support from the US Army Research Office through Grant Number W911NF-21-1-0007.

AUTHOR'S CONTRIBUTION

D.S. and K.B. led the numerical, theoretical and experimental work and co-wrote the manuscript. A.C.D led

the analysis of self-consistent gauge (Appendix A). A.H., I.S., and K.M. provided experimental results. J.E. conceived the project and contributed to all theoretical aspects.

DATA AVAILABILITY STATEMENT

Data and code can be made available on request. Please contact dsannamo@uwaterloo.ca.

[1] J. Emerson, R. Alicki, and K. Życzkowski, *Journal of Optics B: Quantum and Semiclassical Optics* **7**, S347–S352 (2005).

[2] C. Dankert, R. Cleve, J. Emerson, and E. Livine, *Phys. Rev. A* **80**, 012304 (2009).

[3] E. Magesan, J. M. Gambetta, and J. Emerson, *Phys. Rev. Lett.* **106**, 180504 (2011).

[4] E. Magesan, J. M. Gambetta, and J. Emerson, *Phys. Rev. A* **85**, 042311 (2012).

[5] B. Lévi, C. C. López, J. Emerson, and D. G. Cory, *Phys. Rev. A* **75**, 022314 (2007).

[6] J. Helsen, I. Roth, E. Onorati, A. Werner, and J. Eisert, *PRX Quantum* **3**, 020357 (2022).

[7] A. Hashim, L. B. Nguyen, N. Goss, B. Marinelli, R. K. Naik, T. Chistolini, J. Hines, J. Marceaux, Y. Kim, P. Gokhale, T. Tomesh, S. Chen, L. Jiang, S. Ferracin, K. Rudinger, T. Proctor, K. C. Young, I. Siddiqi, and R. Blume-Kohout, *PRX Quantum* **6**, 030202 (2025).

[8] E. Magesan, J. M. Gambetta, B. R. Johnson, C. A. Ryan, J. M. Chow, S. T. Merkel, M. P. da Silva, G. A. Keefe, M. B. Rothwell, T. A. Ohki, M. B. Ketchen, and M. Steffen, *Phys. Rev. Lett.* **109**, 080505 (2012).

[9] A. D. Córcoles, J. M. Gambetta, J. M. Chow, J. A. Smolin, M. Ware, J. Strand, B. L. T. Plourde, and M. Steffen, *Phys. Rev. A* **87**, 030301 (2013).

[10] R. Barends, J. Kelly, A. Megrant, A. Veitia, D. Sank, E. Jeffrey, T. C. White, J. Mutus, A. G. Fowler, B. Campbell, Y. Chen, Z. Chen, B. Chiaro, A. Dunsworth, C. Neill, P. O’Malley, P. Roushan, A. Vainsencher, J. Wenner, A. N. Korotkov, A. N. Cleland, and J. M. Martinis, *Nature* **508**, 500–503 (2014).

[11] J. Kelly, R. Barends, B. Campbell, Y. Chen, Z. Chen, B. Chiaro, A. Dunsworth, A. G. Fowler, I.-C. Hoi, E. Jeffrey, A. Megrant, J. Mutus, C. Neill, P. J. J. O’Malley, C. Quintana, P. Roushan, D. Sank, A. Vainsencher, J. Wenner, T. C. White, A. N. Cleland, and J. M. Martinis, *Phys. Rev. Lett.* **112**, 240504 (2014).

[12] D. C. McKay, S. Sheldon, J. A. Smolin, J. M. Chow, and J. M. Gambetta, *Phys. Rev. Lett.* **122**, 200502 (2019).

[13] J. T. Muhonen, A. Laucht, S. Simmons, J. P. Dehollain, R. Kalra, F. E. Hudson, S. Freer, K. M. Itoh, D. N. Jamieson, J. C. McCallum, A. S. Dzurak, and A. Morello, *Journal of Physics: Condensed Matter* **27**, 154205 (2015).

[14] E. Kawakami, T. Jullien, P. Scarlino, D. R. Ward, D. E. Savage, M. G. Lagally, V. V. Dobrovitski, M. Friesen, S. N. Coppersmith, M. A. Eriksson, and L. M. K. Vandersypen, *Proceedings of the National Academy of Sciences* **113**, 11738–11743 (2016).

[15] J. P. Gaebler, A. M. Meier, T. R. Tan, R. Bowler, Y. Lin, D. Hanneke, J. D. Jost, J. P. Home, E. Knill, D. Leibfried, and D. J. Wineland, *Phys. Rev. Lett.* **108**, 260503 (2012).

[16] H. J. Manetsch, G. Nomura, E. Bataille, X. Lv, K. H. Leung, and M. Endres, *Nature* **647**, 60–67 (2025).

[17] A. J. Weinstein, M. D. Reed, A. M. Jones, R. W. Andrews, D. Barnes, J. Z. Blumoff, L. E. Euliss, K. Eng, B. H. Fong, S. D. Ha, D. R. Hulbert, C. A. C. Jackson, M. Jura, T. E. Keating, J. Kerckhoff, A. A. Kiselev, J. Matten, G. Sabbir, A. Smith, J. Wright, M. T. Rakher, T. D. Ladd, and M. G. Borselli, *Nature* **615**, 817–822 (2023).

[18] S. A. Moses, C. H. Baldwin, M. S. Allman, R. Ancona, L. Ascarrunz, C. Barnes, J. Bartolotta, B. Bjork, P. Blanchard, M. Bohn, J. G. Bohnet, N. C. Brown, N. Q. Burdick, W. C. Burton, S. L. Campbell, J. P. Campora, C. Carron, J. Chambers, J. W. Chan, Y. H. Chen, A. Chernoguzov, E. Chertkov, J. Colina, J. P. Curtis, R. Daniel, M. DeCross, D. Deen, C. Delaney, J. M. Dreiling, C. T. Ertsgaard, J. Esposito, B. Estey, M. Fabrikant, C. Figgatt, C. Foltz, M. Foss-Feig, D. Francois, J. P. Gaebler, T. M. Gatterman, C. N. Gilbreth, J. Giles, E. Glynn, A. Hall, A. M. Hankin, A. Hansen, D. Hayes, B. Higashi, I. M. Hoffman, B. Horning, J. J. Hout, R. Jacobs, J. Johansen, L. Jones, J. Karcz, T. Klein, P. Lauria, P. Lee, D. Liefer, S. T. Lu, D. Lucchetti, C. Lytle, A. Malm, M. Matheny, B. Mathewson, K. Mayer, D. B. Miller, M. Mills, B. Neyenhuis, L. Nugent, S. Olson, J. Parks, G. N. Price, Z. Price, M. Pugh, A. Ransford, A. P. Reed, C. Roman, M. Rowe, C. Ryan-Anderson, S. Sanders, J. Sedlacek, P. Shevchuk, P. Siegfried, T. Skripka, B. Spaun, R. T. Sprenkle, R. P. Stutz, M. Swallows, R. I. Tobey, A. Tran, T. Tran, E. Vogt, C. Volin, J. Walker, A. M. Zolot, and J. M. Pino, *Phys. Rev. X* **13**, 041052 (2023).

[19] Z. Li, P. Liu, P. Zhao, Z. Mi, H. Xu, X. Liang, T. Su, W. Sun, G. Xue, J.-N. Zhang, W. Liu, Y. Jin, and H. Yu, *npj Quantum Information* **9**, 10.1038/s41534-023-00781-x (2023).

[20] Y. Wu, L. Camenzind, P. Bütler, I. Jin, A. Noiri, K. Takeda, T. Nakajima, T. Kobayashi, G. Scappucci, H. Goan, *et al.*, arXiv preprint arXiv:2507.11918.

[21] Y. Song, L. Beltrán, I. Besedin, M. Kerschbaum, M. Pechal, F. m. c. Swiadek, C. Hellings, D. Colao Zanuz, A. Flasby, J.-C. Besse, and A. Wallraff, *Phys. Rev. Appl.* **24**, 024068 (2025).

[22] E. Champion, Z. Wang, R. W. Parker, and M. S. Blok, *Phys. Rev. X* **15**, 021096 (2025).

[23] G. J. Norris, K. Dalton, D. C. Zanuz, A. Rommens, A. Flasby, M. B. Panah, F. Swiadek, C. Scarato, C. Hellings, J.-C. Besse, *et al.*, arXiv preprint arXiv:2503.12603 (2025).

[24] C. Scarato, K. Hanke, A. Remm, S. Lazăr, N. Lacroix, D. Colao Zanuz, A. Flasby, A. Wallraff, and C. Hellings, *PRX Quantum* **6**, 040317 (2025).

[25] Y. Sung, L. Ding, J. Braumüller, A. Vepsäläinen, B. Kanman, M. Kjaergaard, A. Greene, G. O. Samach, C. McNally, D. Kim, A. Melville, B. M. Niedzielski, M. E. Schwartz, J. L. Yoder, T. P. Orlando, S. Gustavsson, and W. D. Oliver, *Phys. Rev. X* **11**, 021058 (2021).

[26] A. Erhard, J. J. Wallman, L. Postler, M. Meth, R. Stricker, E. A. Martinez, P. Schindler, T. Monz,

J. Emerson, and R. Blatt, *Nature Communications* **10**, 10.1038/s41467-019-13068-7 (2019).

[27] J. Emerson, M. Silva, O. Moussa, C. Ryan, M. Laforest, J. Baugh, D. G. Cory, and R. Laflamme, *Science* **317**, 1893–1896 (2007).

[28] D. C. McKay, I. Hincks, E. J. Pritchett, M. Carroll, L. C. Goria, and S. T. Merkel, URL: <http://arxiv.org/abs/2311.05933>.

[29] A. Carignan-Dugas, D. Dahlen, I. Hincks, E. Ospadov, S. J. Beale, S. Ferracin, J. Skanes-Norman, J. Emerson, and J. J. Wallman, arXiv preprint arXiv:2303.17714 (2023).

[30] S. J. Beale, K. Boone, A. Carignan-Dugas, A. Chytros, D. Dahlen, H. Dawkins, J. Emerson, S. Ferracin, V. Frey, I. Hincks, D. Hufnagel, P. Iyer, A. Jain, J. Kolbush, E. Ospadov, J. L. Pino, H. Qassim, J. Saunders, J. Skanes-Norman, A. Stasiuk, J. J. Wallman, A. Winick, and E. Wright, *True-q* (2020).

[31] A. Carignan-Dugas, S. K. Ranu, and P. Dreher, *Quantum* **8**, 1367 (2024).

[32] S. Chen, Y. Liu, M. Otten, A. Seif, B. Fefferman, and L. Jiang, *Nature Communications* **14**, 10.1038/s41467-022-35759-4 (2023).

[33] A. Calzona, M. Papić, P. Figueroa-Romero, and A. Auer, arXiv preprint arXiv:2412.09332 (2024).

[34] Z. Zhang, S. Chen, Y. Liu, and L. Jiang, *PRX Quantum* **6**, 010310 (2025).

[35] S. T. Flammia and J. J. Wallman, *ACM Transactions on Quantum Computing* **1**, 1–32 (2020).

[36] A. Hashim, R. K. Naik, A. Morvan, J.-L. Ville, B. Mitchell, J. M. Kreikebaum, M. Davis, E. Smith, C. Iancu, K. P. O'Brien, I. Hincks, J. J. Wallman, J. Emerson, and I. Siddiqi, *Phys. Rev. X* **11**, 041039 (2021).

[37] N. Fazio, R. Freund, D. Sannamoth, A. Steiner, C. D. Marciak, M. Rispler, R. Harper, T. Monz, J. Emerson, and S. D. Bartlett, arXiv preprint arXiv:2504.11980 (2025).

[38] N. Pulido-Mateo, H. Mendpara, M. Duwe, T. Dubielzig, G. Zarantonello, L. Krinner, and C. Ospelkaus, *Phys. Rev. Res.* **6**, L022067 (2024).

[39] R. Haghshenas, E. Chertkov, M. Mills, W. Kadow, S.-H. Lin, Y.-H. Chen, C. Cade, I. Niesen, T. Begušić, M. S. Rudolph, *et al.*, arXiv preprint arXiv:2503.20870 (2025).

[40] A. Carignan-Dugas, J. J. Wallman, and J. Emerson, *New Journal of Physics* **21**, 053016 (2019).

[41] T. J. Proctor, A. Carignan-Dugas, K. Rudinger, E. Nielsen, R. Blume-Kohout, and K. Young, *Phys. Rev. Lett.* **123**, 030503 (2019).

[42] A. M. Polloreno, A. Carignan-Dugas, J. Hines, R. Blume-Kohout, K. Young, and T. Proctor, *Quantum* **9**, 1848 (2025).

[43] E. Knill, D. Leibfried, R. Reichle, J. Britton, R. B. Blakestad, J. D. Jost, C. Langer, R. Ozeri, S. Seidelin, and D. J. Wineland, *Phys. Rev. A* **77**, 012307 (2008).

[44] K. Boone, A. Carignan-Dugas, J. J. Wallman, and J. Emerson, *Phys. Rev. A* **99**, 032329 (2019).

[45] J. J. Wallman, *Quantum* **2**, 47 (2018).

[46] T. Proctor, K. Rudinger, K. Young, M. Sarovar, and R. Blume-Kohout, *Phys. Rev. Lett.* **119**, 130502 (2017).

[47] T. Proctor, S. Seritan, E. Nielsen, K. Rudinger, K. Young, R. Blume-Kohout, and M. Sarovar, arXiv preprint arXiv:2204.07568 (2022).

[48] B. Foxen, C. Neill, A. Dunsworth, P. Roushan, B. Chiaro, A. Megrant, J. Kelly, Z. Chen, K. Satzinger, R. Barends, F. Arute, K. Arya, R. Babbush, D. Bacon, J. C. Bardin, S. Boixo, D. Buell, B. Burkett, Y. Chen, R. Collins, E. Farhi, A. Fowler, C. Gidney, M. Giustina, R. Graff, M. Harrigan, T. Huang, S. V. Isakov, E. Jeffrey, Z. Jiang, D. Kafri, K. Kechedzhi, P. Klimov, A. Korotkov, F. Kostritsa, D. Landhuis, E. Lucero, J. McClean, M. McEwen, X. Mi, M. Mohseni, J. Y. Mutus, O. Naaman, M. Neeley, M. Niu, A. Petukhov, C. Quintana, N. Rubin, D. Sank, V. Smelyanskiy, A. Vainsencher, T. C. White, Z. Yao, P. Yeh, A. Zalcman, H. Neven, and J. M. Martinis (Google AI Quantum), *Phys. Rev. Lett.* **125**, 120504 (2020).

[49] S. Merkel, T. Proctor, S. Ferracin, J. Hines, S. Barron, L. C. Goria, and D. McKay, arXiv preprint arXiv:2503.05943 (2025).

[50] J. M. Gambetta, A. D. Córcoles, S. T. Merkel, B. R. Johnson, J. A. Smolin, J. M. Chow, C. A. Ryan, C. Rigetti, S. Poletto, T. A. Ohki, M. B. Ketchen, and M. Steffen, *Phys. Rev. Lett.* **109**, 240504 (2012).

[51] M. A. Nielsen, *Physics Letters A* **303**, 249–252 (2002).

[52] A. Carignan-Dugas, M. Alexander, and J. Emerson, *Quantum* **3**, 173 (2019).

[53] J. Wallman, C. Granade, R. Harper, and S. T. Flammia, *New Journal of Physics* **17**, 113020 (2015).

[54] A. Carignan-Dugas, K. Boone, J. J. Wallman, and J. Emerson, *New Journal of Physics* **20**, 092001 (2018).

[55] A. W. Knapp (1988).

[56] D. C. McKay, C. J. Wood, S. Sheldon, J. M. Chow, and J. M. Gambetta, *Phys. Rev. A* **96**, 022330 (2017).

[57] N. Fruitwala, A. Hashim, A. D. Rajagopala, Y. Xu, J. Hines, R. K. Naik, I. Siddiqi, K. Klymko, G. Huang, and K. Nowrouzi, arXiv preprint arXiv:2406.13967 (2024).

[58] J. M. Pino, J. M. Dreiling, C. Figgatt, J. P. Gaebler, S. A. Moses, M. S. Allman, C. H. Baldwin, M. Foss-Feig, D. Hayes, K. Mayer, C. Ryan-Anderson, and B. Neyenhuis, *Nature* **592**, 209–213 (2021).

[59] J. J. Wallman and J. Emerson, *Phys. Rev. A* **94**, 052325 (2016).

[60] M. Ishii, H. Qassim, T. Kurita, J. Emerson, K. Maruyama, H. Oshima, and S. Sato, arXiv preprint arXiv:2503.05344 (2025).

[61] T. Kurita, H. Qassim, M. Ishii, H. Oshima, S. Sato, and J. Emerson, *Quantum* **7**, 1184 (2023).

[62] J.-L. Ville, A. Morvan, A. Hashim, R. K. Naik, M. Lu, B. Mitchell, J.-M. Kreikebaum, K. P. O'Brien, J. J. Wallman, I. Hincks, J. Emerson, E. Smith, E. Younis, C. Iancu, D. I. Santiago, and I. Siddiqi, *Phys. Rev. Res.* **4**, 033140 (2022).

[63] A. Winick, J. J. Wallman, D. Dahlen, I. Hincks, E. Ospadov, and J. Emerson, arXiv preprint arXiv:2212.07500 (2022).

[64] Y. Gu, Y. Ma, N. Forcellini, and D. E. Liu, *Phys. Rev. Lett.* **130**, 250601 (2023).

[65] M. Urbanek, B. Nachman, V. R. Pascuzzi, A. He, C. W. Bauer, and W. A. de Jong, *Physical review letters* **127**, 270502 (2021).

[66] P. K. Faehrmann, M. Steudtner, R. Kueng, M. Kieferova, and J. Eisert, *Quantum* **6**, 806 (2022).

[67] P. Iyer, A. Jain, S. D. Bartlett, and J. Emerson, *Phys. Rev. Res.* **4**, 043218 (2022).

- [68] A. Jain, P. Iyer, S. D. Bartlett, and J. Emerson, [Improved quantum error correction with randomized compiling](#) (2023).
- [69] P. Iyer, A. Jain, S. D. Bartlett, and J. Emerson, arXiv preprint arXiv:2507.08536 (2025).

Appendix A: Construction of the Self-Consistent Gauge

In numerical studies of randomized benchmarking, the simple and standard approach is to assign an error to each gate, which can generally be gate-dependent. From this one can define a fidelity (or infidelity) associated with an average over the fidelities (or infidelities) associated with each of these noisy gates. This is the ‘error-on-the gate’ approach to defining a “theoretical infidelity” for the numerical simulation. However, the error rate measured by RB is the average ‘error-between-the-gates’ of the randomized sequence [45], which can differ from the naive approach because it accounts for the possibility of coherent combination of the errors from sequential gates, i.e., between the error on any one gate and the error on the subsequent gate. Taking this into account resolves the concern raised in [46] about that RB actually measures.

For historical reasons, the above issues are normally discussed as a gauge freedom in defining the theoretical fidelity. For historical continuity, we follow this framework to ask and answer the following question: if we measure a fidelity from a numerical experiment such as RB, how can we compare it to a rigorous theoretical value associated with the error model when the relevant error is the average error-between-the gates? There is a rather simple way to answer this question, which we call the self-consistent gauge (SCG) fidelity.

Consider a set of noisy state representations $\{ |\tilde{\rho}_i\rangle\langle\tilde{\rho}_i| \}$, a set of noisy measurement representations $\{ \langle\tilde{\mu}_i | \}$, and a set of noisy superoperators $\{ \tilde{G}_i \}$. With these vectors and matrices we can express the probability of outcome k given any sequence of operators $\tilde{G}_{j_m} \cdots \tilde{G}_{j_1}$ applied on any state $\tilde{\rho}_i$:

$$p(\text{outcome } k | \text{operations} = [j_m, \dots, j_1], \text{state } i) = \langle\langle \tilde{\mu}_k | \tilde{G}_{j_m} \cdots \tilde{G}_{j_1} | \tilde{\rho}_i \rangle\rangle. \quad (\text{A1})$$

These probabilities are the only physically measurable quantities, therefore the sets $\{ S | \tilde{\rho}_i \rangle\langle\tilde{\rho}_i | \}$, $\{ \langle\tilde{\mu}_i | S^{-1} \}$, and $\{ S \tilde{G}_i S^{-1} \}$ describe the same physical observations (here S could be any $d^2 \times d^2$ invertible matrix).

In light of this gauge freedom, it has been proposed [46] that the process fidelity should actually be expressed in the following gauge-dependent form:

$$f(S \tilde{G}_i S^{-1}, G_i) = \frac{\text{Tr}(S \tilde{G}_i S^{-1} G_i^{-1})}{d^2}, \quad (\text{A2})$$

which depends on the gauge matrix S . Without endorsing the correctness of this general claim, we adopt this framework because it is general enough to accommodate the analysis of the difference between the ‘error-on-the-gate’ model that defines the theoretical fidelity and the effective ‘error-between-the-gates’ that determined the observed fidelity in numerical simulations.

Now we get to the crux of the issue: consider the simple case where noisy gates take the form

$$\tilde{G}_i = L G_i R \quad \forall \tilde{G}_i \in \{ \tilde{G}_i \}, \quad (\text{A3})$$

where L and R are left and right error channels respectively. In such scenario, the probability of outcome k given any sequence of operators $\tilde{G}_{j_m} \cdots \tilde{G}_{j_1}$ applied on any state $\tilde{\rho}_i$ takes the form:

$$\begin{aligned} p(\text{outcome } k | \text{operations} = [j_m, \dots, j_1], \text{state } i) \\ = \langle \langle \tilde{\mu}_k | LG_{j_m} R LG_{j_{m-1}} \cdots G_2 R LG_{j_1} R | \tilde{\rho}_i \rangle \rangle. \end{aligned} \quad (\text{A4})$$

Since the initial R and last L can be factored in state preparation and measurement errors, it becomes quite obvious that RB will provide an estimate of the process fidelity of RL to the identity, $f(RL)$. On the other hand, the process fidelity averaged over the Cliffords is expressed as

$$\begin{aligned} \mathbb{E}_{\substack{G_i \\ \text{is Clifford}}} \frac{\text{Tr}(SLG_i RS^{-1} G_i^{-1})}{d^2} = f(SL)f(RS^{-1}) \\ + O(r(SL)r(RS^{-1})). \end{aligned} \quad (\text{A5})$$

Therefore, the RB fidelity gets in good agreement with the average fidelity obtained in the gauge S as long as

$$f(RL) = f(SL)f(RS^{-1}) + O(r(SL)r(RS^{-1})). \quad (\text{A6})$$

Two obvious choices are $S = R$ and $S = L^{-1}$, but let's explore options of S that are constrained to physical unitaries. Suppose that R is *decoherent* as defined in [52]. That is, the leading Kraus operator of R is positive semi-definite. As shown in [52], it follows that the composite fidelity is multiplicative: $f(RL) = f(R)f(L) + O(r(R)r(L))$. In such case, the choice $S = I$ (i.e. no gauge transformation) satisfies Eqn. A6. Now, let's express $R = U_R D_R$ and $L = U_L D_L$ where U_R, U_L are physical unitary channels and D_R, D_L are physical decoherent channels. This polar decomposition is always possible for high-enough fidelity channels, as shown in [52].

Moreover, there is a constructive way to find the polar decomposition of a channel Λ close to the identity:

1. Express Λ in its Choi matrix representation Λ_{Choi} .
2. The eigenvalues of Λ_{Choi} can be interpreted as probabilities, and the eigenvectors are vectorized Kraus operators. Since Λ is close to the identity, there is an eigenvalue of Λ_{Choi} that is close to 1. Its corresponding Kraus operator is the leading Kraus operator K_0 .
3. Perform a standard polar decomposition $K_0 = UP$ where U is a $d \times d$ unitary, and P is $d \times d$ a positive semi-definite matrix. Let \mathcal{U} be the superoperator version of U .
4. $\Lambda = \mathcal{U}D$ where $D := \mathcal{U}^\dagger \Lambda$ is purely decoherent.

Leveraging fidelity composition rules with decoherent

channels, we get

$$\begin{aligned} f(RL) &= f(D_R)f(D_L)f(U_R U_L) \\ &+ O(r(D_R)r(D_L)U_R U_L) + O(r(D_L)r(U_R U_L)), \end{aligned} \quad (\text{A7})$$

$$f(SL) = f(D_L)f(SU_L) + O(r(SU_L)r(D_L)), \quad (\text{A8})$$

$$f(RS^{-1}) = f(D_R)f(U_R S^{-1}) + O(r(U_R S^{-1})r(D_R)). \quad (\text{A9})$$

Substituting those in Eqn. A6 and omitting the second order terms (s.o.t), we get the condition

$$f(U_R U_L) = f(U_R S^{-1})f(SU_L) + \text{s.o.t.}, \quad (\text{A10})$$

meaning that $S = U_R$ or $S = U_L^{-1}$ satisfy Eqn. A6. In other words, if we are given the simple noise model $\tilde{G}_i = U_L D_L G_i U_R D_R$, the average gate set fidelities of $\{U_L^\dagger \tilde{G}_i U_L\}$ and of $\{U_R \tilde{G}_i U_R^\dagger\}$ are in good agreement with the reported RB number.

It is now time to depart from the simple noise model $\tilde{G}_i = LG_i R$ (Eqn. A3). To do so, we will need to consider gate sets that are groups. As we shall see, we define a gauge-fixing method for any given group \mathbb{G} as long as it forms a t -design for $t \geq 1$. First, it has been shown that given such group \mathbb{G} , there exist L and R (independent of S) such that;

$$\mathbb{E}_{G_i \in \mathbb{G}} G_i^{-1} (RS^{-1}) (S \tilde{G}_i S^{-1}) = \Lambda^{\mathbb{G}} RS^{-1}, \quad (\text{A11})$$

$$\mathbb{E}_{G_i \in \mathbb{G}} (S \tilde{G}_i S^{-1}) (SL) G_i^{-1} = SL \Lambda^{\mathbb{G}}, \quad (\text{A12})$$

where $\Lambda^{\mathbb{G}}$ is a channel twirled by the group \mathbb{G} and is independent of S . It is shown in [45] that the decaying fidelities extracted by CB-like and RB-like protocols are the fidelities of $\Lambda^{\mathbb{G}}$. To understand what the fidelities of $\Lambda^{\mathbb{G}}$ correspond to, first notice that L and R can be approximated up to second order terms (s.o.t.) in the infidelities by the following physical channels [54]:

$$L = \underbrace{\mathbb{E}_{G_i \in \mathbb{G}} \tilde{G}_4 \tilde{G}_3 \tilde{G}_2 \tilde{G}_1 (G_4 G_3 G_2 G_1)^{-1}}_{=: \mathcal{E}_L} + \text{s.o.t.} \quad (\text{A13})$$

$$R = \underbrace{\mathbb{E}_{G_i \in \mathbb{G}} (G_4 G_3 G_2 G_1)^{-1} \tilde{G}_4 \tilde{G}_3 \tilde{G}_2 \tilde{G}_1}_{=: \mathcal{E}_R} + \text{s.o.t.} \quad (\text{A14})$$

Why 4? Because the eigenvalues of the twirl super-duper operator $T_{\mathbb{G}} := \mathbb{E}_{G_i \in \mathbb{G}} G_i^* \otimes \tilde{G}_i$ are either close to 1 or at most $O(\sqrt{r_i})$, meaning that concatenating this twirl 4 times brings $O(\sqrt{r_i})$ to $O(r_i^2)$ (here r_i refers to infidelities).

Similarly as earlier, let's decompose $\mathcal{E}_L = U_L D_L$ and $\mathcal{E}_R = U_R D_R$ where U_R, U_L are physical unitary channels and D_R, D_L are physical decoherent channels. Substituting these into Eqns. A11 and A12, and taking the fidelity on each side, we obtain:

$$\begin{aligned} f \left(\left[\mathbb{E}_{G_i \in \mathbb{G}} S \tilde{G}_i S^{-1} G_i^{-1} \right] [U_R D_R S^{-1}] \right) = \\ f(\Lambda^{\mathbb{G}}) f(U_R D_R S^{-1}) + \text{s.o.t.}, \end{aligned} \quad (\text{A15})$$

$$\begin{aligned} f \left(\left[\mathbb{E}_{G_i \in \mathbb{G}} (G_i^{-1} S \tilde{G}_i S^{-1}) \right] [SU_L D_L] \right) = \\ f(\Lambda^{\mathbb{G}}) f(SU_L D_L) + \text{s.o.t.} \end{aligned} \quad (\text{A16})$$

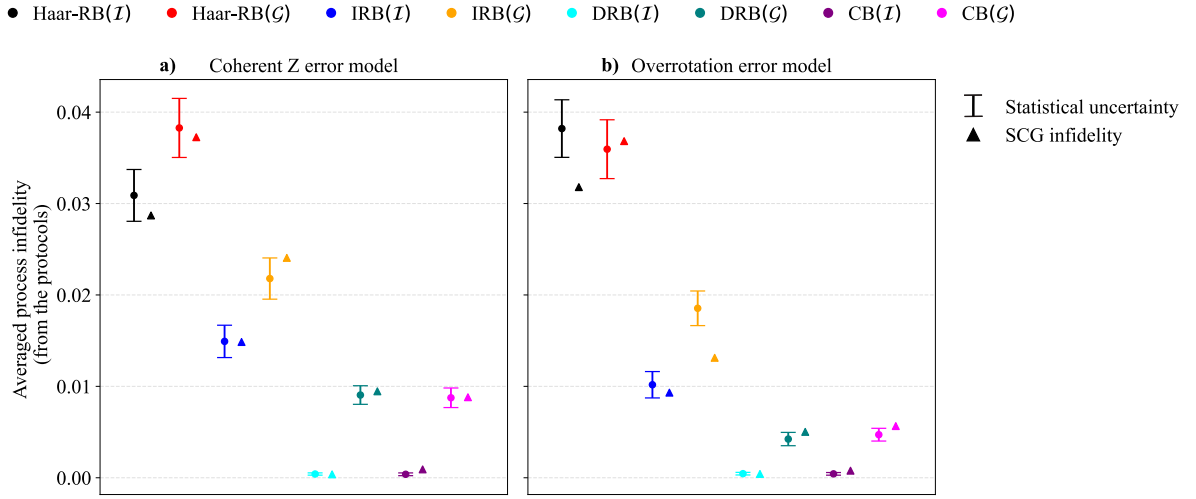


FIG. 7. Numerical plots showing that the estimate of the process infidelities obtained from the different protocols closely matches the self-consistent gauge infidelity values. (a) Error model with two-qubit gates error of the form $e^{i\theta_2 ZZ}$ with $\theta_2 = 10^\circ$ and single qubit gates having fixed gate error of the form $e^{i\theta_1 Z}$ with $\theta_1 = 1^\circ$. (b) Error model of the form $U^{1+\delta}$ where U is the unitary on which noise is applied. For two qubit gates $\delta = 0.05$ and for single qubit gates $\delta = 0.01$. The triangles beside each estimate are obtained using the self-consistent gauge for that experiment as discussed in A. The twirling group for finding the self-consistent gauge is similar to the twirling group for each protocol beside which it is plotted.

This means that choosing either $S = U_R$ or $S = U_L^{-1}$ yield to a good agreement between the experimentally-obtained average decay and the average fidelity:

$$\mathbb{E}_{G_i \in \mathbb{G}} f(S\tilde{G}_i S^{-1}, G_i) = f(\Lambda^{\mathbb{G}}) + \text{s.o.t.} \quad (\text{A17})$$

In summary, the gauge-fixing method that we propose to obtain an agreement between experimentally-obtained values and the average fidelity of a group \mathbb{G} is:

1. Find or approximate \mathcal{E}_R and \mathcal{E}_L as defined in Eqns. A11 and A12. The approximation can be done by sampling rather than taking the entire average.
2. Decompose $\mathcal{E}_L = U_L D_L$ and $\mathcal{E}_R = U_R D_R$ where U_R, U_L are physical unitary channels and D_R, D_L are physical decoherent channels. We explain how to do this polar decomposition earlier in this section.
3. Choose either $S = U_R$ or $S = U_L^{-1}$.

We followed this method to plot the triangles which denote the “self-consistent gauge” (SCG) infidelity in Fig. 7.

Appendix B: Estimating the process infidelity of the interleaved gate

When the twirling group is Clifford, the estimator for the process infidelity of the interleaved gate can be constructed from the single decay parameters for each of the interleaved sequence and the reference sequence [8]. In

this case the estimator for the process infidelity of the error acting on the interleaved gate is given by

$$\hat{\epsilon}^{\mathcal{F}} = \frac{d^2 - 1}{d^2} \left(1 - \frac{p^{\mathcal{E} \circ \mathcal{F}}}{p^{\mathcal{E}}} \right) \quad (\text{B1})$$

Using the relation of $p = 1 - \frac{d^2}{d^2 - 1} \epsilon$ [40], the above equation can be rewritten as

$$\hat{\epsilon}^{\mathcal{F}} = \frac{\epsilon^{\mathcal{E} \circ \mathcal{F}} - \epsilon^{\mathcal{E}}}{1 - \frac{d^2}{d^2 - 1} \epsilon^{\mathcal{E}}} \quad (\text{B2})$$

which under expansion up to second order terms gives

$$\hat{\epsilon}^{\mathcal{F}} = \epsilon^{\mathcal{E} \circ \mathcal{F}} - \epsilon^{\mathcal{E}} + \frac{d^2}{d^2 - 1} \epsilon^{\mathcal{E} \circ \mathcal{F}} \epsilon^{\mathcal{E}} - \frac{d^2}{d^2 - 1} (\epsilon^{\mathcal{E}})^2 + O(\epsilon^3) \quad (\text{B3})$$

However not all interleaved benchmarking schemes do admit a single decay parameter ‘ p ’ because the twirling group need not be a unitary 2-design [2]. This motivates the need for a unified and protocol-independent estimator for the process infidelity of the error on the interleaved gate. For such protocols, we begin with the observation that an estimator for the process fidelity of the interleaved gate is given by

$$\hat{F}_p^{\mathcal{F}} = F_p^{\mathcal{E} \circ \mathcal{F}} / F_p^{\mathcal{E}} \quad (\text{B4})$$

where $F_p^{\mathcal{E}}$ and $F_p^{\mathcal{F}}$ are the observed process fidelities of the cycle of randomizing gates and interleaved gate respectively. We now show that this estimator is negligibly different from that proposed originally in IRB. Writing the estimator for process fidelity $\hat{F}_p = 1 - \hat{\epsilon}$, we obtain

$$\hat{\epsilon}^{\mathcal{F}} = 1 - \frac{1 - \epsilon^{\mathcal{E} \circ \mathcal{F}}}{1 - \epsilon^{\mathcal{E}}} \quad (\text{B5})$$

which reproduces Eqn. 2. Expanding Eqn. B5 expression up to second order terms gives

$$\hat{\epsilon}^{\mathcal{F}} = \epsilon^{\mathcal{E} \circ \mathcal{F}} - \epsilon^{\mathcal{E}} + \epsilon^{\mathcal{E} \circ \mathcal{F}} \epsilon^{\mathcal{E}} - (\epsilon^{\mathcal{E}})^2 + O(\epsilon^3) \quad (\text{B6})$$

Comparing Eqn. B3 and Eqn. B6, we observe that the two expressions are identical to each other up to the second order terms except the presence of the prefactor $\frac{d^2}{d^2-1}$.

To quantify the difference when the twirling group is Clifford, we compare the two estimators for the error models used in our numerical studies. For the coherent Z error model, using Eqn. 2 we get $\epsilon^{\mathcal{F}} = 6.978(2.901) \times 10^{-3}$ and using Eqn. B2, we get $\epsilon^{\mathcal{F}} = 6.985(2.904) \times 10^{-3}$. Similarly, for the overrotation error model, using Eqn. 2 we get $\epsilon^{\mathcal{F}} = 8.450(2.397) \times 10^{-3}$ and using Eqn. B2, we get $\epsilon^{\mathcal{F}} = 8.456(2.398) \times 10^{-3}$. In both cases, the discrepancy between the two estimators is on the order of $O(10^{-6})$, which is negligible compared to the statistical uncertainty. This demonstrates that estimating the interleaved gate infidelity via Eqn. 2 provides a consistent and accurate approach, while remaining applicable to a general class of interleaved benchmarking protocols.